International Journal of Thermal Sciences 65 (2013) 242–253

Contents lists available at SciVerse ScienceDirect

International Journal of Thermal Sciences

journal homepage: www.elsevier.com/locate/ijts

Analysis of the hot-disk technique applied to low-density insulating materials

R. Coquard [a,*], E. Coment [b,1], G. Flasquin [b,1], D. Baillis [c,2]

[a] Société "Etude Conseils Calcul en Mécanique des Structures" (EC2MS), 66, boulevard Niels Bohr, 69603 Villeurbanne Cedex, France
[b] Société NEOTIM, MDI – ZA Albitech, 54 rue Gustave Eiffel, 81000 Albi, France
[c] Laboratoire de Mécanique des Contacts et des Solides (LAMCOS), UMR CNRS/INSA Lyon 5514, 20 rue des Sciences, 69621 Villeurbanne Cedex, France

ARTICLE INFO

Article history:
Received 25 November 2011
Received in revised form
11 October 2012
Accepted 13 October 2012
Available online 17 November 2012

Keywords:
Hot-disk technique
Radiation-conduction coupling
Thermally active probe
Low-density insulators

ABSTRACT

The hot-disk technique is a very practicable transient method of measurement of the thermal properties of solid materials. It has been applied successfully to a wide variety of materials. However, it is based on several approximations regarding the nature of the heat transfer. Notably, the probe is considered thermally neutral, and the heat transfer is assumed purely conductive. These two assumptions are questionable when dealing with low-density thermal insulators. In order to evaluate the accuracy of the method, we have generated numerically noised thermograms reproducing the thermal response that would be recorded when measurements are applied to those type of materials. Thereafter, the best-fitting procedure of the classical hot-disk technique was applied to these thermograms. The analysis of the identification results show that the presence of a radiative contribution do not affect the accuracy of the thermal properties identified. The conductivity measured actually corresponds to the equivalent conductivity. On the other hand, when the method is applied to materials with thermal inertia strongly different from the probe ($\approx$2 order of magnitude lower or more), the accuracy of the method becomes questionable. This is notably the case for common insulators used in the building industry like polymer foam or mineral wools. The preceding conclusions have been validated by experimental measurements on a standard low-density XPS foam sample and a superinsulating silica areogel.

1. Introduction

The accuracy of thermal conductivities measurement takes on particular importance in numerous physical, chemical or medical applications given that it has a direct influence on the estimation of heat losses, or temperature rise. The standard measuring method for the thermal conductivity is the so-called "guarded hot-plate method". The principle is to measure the heat flux passing through a slab of materials subjected to a one dimensional steady state heat transfer. This technique gives very accurate results. Nevertheless, it is restricting given that the slab must have large and standard dimensions and that it requires especially long measuring durations.

To remedy these drawbacks, experimental methods of measurement of thermophysical properties based on transient measurements have been developed during the last two decades. As example, the FLASH method [1–3] has been extensively used on a broad range of materials. The validity of this method for the estimation of the equivalent thermal conductivity of semi-transparent foam has been recently demonstrated [4]. Another common transient method used for the measurement of thermal conductivity is the so-called hot-wire method. It is relatively simple and fast as it is based on the measurement of the temperature rise of a uniformly heated wire located inside a sample with any shape and relatively small size. It has been used in numerous studies dealing with solid and pasty thermal insulators [5], soil [6] or thin plates [7] and gives satisfactory results. However, as the method is based on the Fourier diffusion law, it is theoretically not applicable to materials where radiative heat transfer occurs and then, it is restricted to opaque or ideally transparent materials. However, according to Coquard et al. [8], the method could be generalized to semi-transparent materials under certain conditions regarding the dimensions of the apparatus.

More recently, a new transient method called transient plane source (TPS) technique or "hot-disk" technique has been proposed for thermal transport studies of solid materials [9,10]. This transient plane source method is based on the heating of a plane double resistive spiral sandwiched between two samples of the material to be characterized. The recording of the mean temperature of the

* Corresponding author. Tel.: +33 4 37 48 84 37; fax: +33 4 37 48 84 05.
E-mail addresses: remi.coquard@ec2-ms.fr, remi.coquard@ec2-modelisation.fr (R. Coquard), coment@neotim.fr (E. Coment), dominique.baillis@insa-lyon.fr (D. Baillis).
[1] Tel.: +33 5 63 38 05 39; fax: +33 5 63 48 14 30.
[2] Tel.: +33 4 72 43 84 74.

1290-0729/$ – see front matter © 2012 Elsevier Masson SAS. All rights reserved.
http://dx.doi.org/10.1016/j.ijthermalsci.2012.10.008

Nomenclature

a	thermal diffusivity of the material (m^2/s)
A	constant temperature jump of the probe due to non-perfect thermal contact (K)
C	Specific Heat of the material (J/kg/K)
D	distance traveled by the heating during the measurement time (m)
r_0	radius of the hot-disk probe (m)
e	total thickness of the hot-disk probe (m)
e_{Ni}	thickness of the Nickel spiral immersed in the probe (m)
g	spectral asymmetry factor of the phase function
$I(r,z,\theta,\varphi)$	radiant intensity at the point (r,z) in the direction (θ,φ) ($W/m^2/Sr$)
$I_{i,j}^m$	radiant intensity at the discrete point (r_i,z_j) in the discrete direction m ($W/m^2/Sr$)
$I_0(T)$	radiant intensity of the black body at temperature T ($W/m^2/Sr$)
k	thermal conductivity of the material (W/m/K)
k_{equ}	"equivalent" conductivity of the material (W/m/K)
L	space interval between hot and cold plates for the computation of $k_{equ,num}$ (m)
N	number of measurement points
No	relative amplitude of the noise
$P(\theta)$	scattering phase function
q	heat flux density (W/m^2)
$\dot{Q}$	volumetric heat flux generated in the probe by Joule effect (W/m^3)
$Q = U.I$	heat flux generated in the probe by Joule effect (W)
r	radial coordinate (m)
R	electrical resistance (Ω)
R_c	thermal contact resistance (m^2 K/W)
t	time (s)
t_c	time correction (s)
T	temperature (K)
T_{ext}	temperature of the surrounding environment (K)
V	volume (m^3)
w_m	weighting factor for the mth direction of the angular discretization
z	axial coordinate

Greek symbols

β, σ and κ	extinction, scattering and absorption coefficients (m^{-1})
Δt	time increment (s)
$\Delta T = T - T_{ext}$	temperature increase (K)
ε_h, ε_c, ε_p	emissivity of the hot plate, cold plate and of the probe
Ω	solid angle
λ	radiation wavelength (μm)
$\mu = \sin\theta.\cos\phi, \xi = \cos\theta, \eta = \sin\theta.\sin\varphi$	direction cosines of the radiant intensity
ρ	density of the material (kg/m^3)
σ_{SB}	Stefan–Boltzmann constant ($\approx 5.67.10^{-8}$ $W/m^2/K^4$)
$\tau = \sqrt{a.t/r_0^2}$	dimensionless time
$\omega = \sigma/\beta$	scattering albedo

Subscripts

c	conductive
exp	experimental
G	generated numerically
i,j	at the point of coordinates r_i,z_j
$ident$	identified
Ka	Kapton
min, max	minimum, maximum values
Ni	Nickel spiral
num	numerical
p	of the probe
r	radiative
t	total
th	theoretical
λ	spectral value

Superscripts

l	at the lth iteration
m	mth direction of the quadrature
r	along the radial axis
z	along the z-axis

heating element combined with a parameter estimation method makes it possible to estimate thermal conductivity and thermal diffusivity of the samples from a single experiment. The method is rapid and very practical since no particular shape is required for the sample tested and the size of this sample is relatively limited. In addition to its rapidity and ease of use, the main advantage of this technique is the possibility to determine both the thermal conductivity and the thermal diffusivity from one single transient measurement. This technique gave rise to the commercialization of a "hot disk" thermal constants analyzer generally referred as "hot-disk". This probe is, at the moment, extensively used due to its claimed ability to produce accurate estimations for a large variety of solids and liquids. The hot-disk analyzer was studied and used by numerous authors [11–16].

Bohac et al. [11] improved the accuracy of the method by computing the sensitivity coefficients for the thermal diffusivity and conductivity. From the analysis of these coefficients, they proposed optimal time window to be used for determining both the thermal conductivity and the thermal diffusivity. This time window has been validated using experimental results on Perspex and stainless steel for both the thermal conductivity and the thermal diffusivity.

Gustavsson and Gustafsson [17] also proposed a modification of the fitting procedure used in the hot-disk technique in order to improve the accuracy of the measured thermal properties. It consists in incorporating two additional model-fitted variables in the direct model: a constant temperature increase component A reproducing the total thermal contact resistance and a time correction t_c. By using these two additional parameters, the disturbing influence of the bad thermal contact between the probe and the material as well as the inertia of the probe are significantly reduced allowing a better estimation of the thermal conductivity and diffusivity of the material by the hot-disk measurement.

Recently, Jannot and Acem [15] have developed a complete model based on the thermal quadrupoles formalism to represent the hot disc temperature variation taking into account both the thermal inertia of the probe and possible contact resistance between the solid to be characterized and the probe. This model permits them to show that the reliability of the measurements obtained by the hot-disk technique might be questionable in some particular cases where (1) the thermal contact resistance or (2) the thermal inertia of the hot disc, could not be neglected as it is assumed in the standard analysis. However, it can be noticed that their model did not take into account the real thermal conductivity

of the probe and thus, they were not able to quantify the effect of this deviation from the ideal case.

The studies, discussed just above, which have been interested in the analysis of the limitations and restrictions in the use of the hot-disk analyzers are very scarce. This could appear quite surprising since one of the main strength of the method is precisely its large field of application (the fields of commercial application claimed by the manufacturer are 0.005–500 W/m/K for the thermal conductivity, 0.1 to 100 $\times$ 10^{-6} m^2/s for the thermal diffusivity and 30 K–1000 K for the temperature). However, in addition to the thermal influence of the probe and to the possible contact resistance between the disk and the material, the existence of other modes of heat transfer along with the thermal conduction might also disturb the transient plane source measurements and influence the values of the thermal properties estimated by the fitting procedure. Then, although the hot-disk method has been largely used with apparent satisfaction for a wide range of materials and temperatures, there remain, from a theoretical point of view, some uncertainties about its applicability and accuracy for low-density materials in which radiative heat transfer could be significant.

Therefore, the aim of the present study is to estimate the reliability of the hot-disk technique for low-density thermal insulators for which non-ideal conditions are encountered: (1) thermally non-neutral probe due to its thermal capacity ($\rho_p.C_p \neq \rho.C$) or thermal conductivity ($k_p \neq k$); (2) presence of significant radiative heat transfer in the material analyzed (semi-transparent material). To fulfil these objectives, we have developed a numerical model based on the resolution of the coupled (radiation–conduction) heat transfer problem around realistic thermally active probes. This model uses a combination of the Finite Volume Method (FVM) and the Discrete Ordinates Method (DOM). It has been used to generate numerically noised thermograms that would be recorded using existing probes on various low-density semi-transparent insulating materials with realistic radiative and conductive properties. The modeling of heat transfer inside the probe has been developed to take into account as faithfully as possible the composite structure of existing probes. Thereafter, a least square fit-method associated with an analytical simulation of the purely conductive heat transfer around the probe taking into account the constant component A and the time correction t_c has been applied to these thermograms. It allows evaluating the errors made on the thermal properties of low-density thermal insulators estimated using the classical hot-disk fitting procedure. This also permits us to underline and quantify the critical conditions under which the reliability of the hot-disk measurements should be questioned for this type of materials. Thereafter, we conducted a campaign of hot-disk measurements on various thermal insulators samples which allowed us to validate the theoretical conclusions.

2. Theoretical considerations

2.1. Principle of the hot disk thermal constants analyzer

The hot disk thermal constants analyzer (HD), manufactured by hot disk AB, utilizes a sensor element in the shape of a double spiral which acts both as a heat source for increasing the temperature of the sample and an "Ohmic resistance thermometer" (Wheatstone bridge) for recording the time-dependent temperature increase. The spiral, made of nickel covered on both sides with Kapton for protection and electrical insulation is simply placed between two halves of the sample tested.

From a theoretical point of view, the increase of the probe temperature is obtained by solving the conduction equation assuming that the hot disk consists of n concentric ring heat sources located in an infinitely large sample. If we also assume that the thermal contacts are perfect and that hot-disk probe is thermally neutral (thermal properties identical to the material tested), the time-dependent temperature increase is given by:

$$\Delta T_{th}(t) = \frac{Q}{\pi^{3/2}.r_0.k} D_n(\tau) \tag{1}$$

With

$$\tau = \sqrt{a.t/r_0^2}, D_n(\tau) = [n.(n+1)]^{-2} \int_0^{\tau} \left[\sigma^{-2} \sum_{l=1}^{n} \sum_{k=1}^{n} l.k.\exp \times \left(-\frac{l^2+k^2}{4.n^2.\sigma n} \right) I_0\left(\frac{lk}{2.n^2.\sigma n} \right) \right] .d\sigma$$

and I_0 is the modified Bessel Function of the first kind of order zero.

When performing a measurement with the hot disk method, the temperature response includes the two additional parameters A and t_c introduced by Gustavsson and Gustafsson [17]. Then, ΔT is a sum of two components, one component which is essentially constant (A) and the transient component:

$$\Delta T_{th}(t) = A + \frac{Q}{\pi^{3/2}.r_0.k} D_n(\tau') \tag{2}$$

with

$$\tau' = \sqrt{a.(t-t_c)/r_0^2}$$

The term A is supposed to group the influence of non-perfect thermal contact while the time correction t_c is expected to take into account other non-ideal conditions such as the thermal inertia of the probe and the non-instantaneous establishment of the heating power.

When the number of concentric rings is very important ($n \to \infty$), the term $D_n(\tau)$ can be expressed more simply:

$$D_{\infty}(\tau) = \int_0^{\tau} \int_0^1 \int_0^1 \frac{u.v}{\sigma^2} .\exp\left(-\frac{u^2+v^2}{4.\sigma^2} \right) .I_0\left(\frac{u.v}{2.\sigma^2} \right) .du.dv.du. \tag{3}$$

The increase of the temperature of the probe is measured experimentally from the variations of the electrical resistance of the probe using the following relation:

$$R(t) = R_0.(1+\alpha.\Delta T_{\exp}(t)) \Rightarrow \Delta T_{\exp}(t) = \frac{R(t)-R_0}{\alpha.R_0} \tag{4}$$

where R_0 (Ω) is the initial electrical resistance and $\alpha(K^{-1})$ is the temperature coefficient of resistivity of the probe

A curve fitting procedure is then applied to the thermograms recorded experimentally in order to estimate the values of the thermal conductivity and diffusivity as well as the parameters A and t_c which minimize the differences between the experimental ΔT_{exp} and theoretical ΔT_{th} variations of the temperature. In practice, a minimum sample size is required given that the distance traveled by the heating referred as "probing depth" must not exceed the available sample size in order to avoid "side effects". This "probing depth" can be estimated by $D \approx 2.\sqrt{(a.t)}$. This leads to an optimal time interval $[0; t_{\max}]$ proposed by the manufacturer for the application of the parameter estimation.

2.2. Numerical modeling of the hot-disk measurement

We have developed a numerical model taking into account the entire phenomenon actually neglected in the analytical model used

for the parameter estimation process (Eq. (1)) of the classical hot-disk measurement technique, i.e., the thermal influence of the probe, the contact resistance and the presence of radiative heat transfer. This axisymmetric model is based on a combination of the Finite Volume Method (FVM) and the Discrete Ordinates Method (DOM). These methods consist in the computation of the temperature field ($T(r,z)$) and intensity field $I(r,z,\theta,\varphi)$ in the semi-transparent surrounding medium and in the circular opaque probe ($T_p(r,z)$). The circular probe taken into account in the model is shown on Fig. 1 and reproduces as realistically as possible the structure of existing probes. They are actually composed of a thin Nickel spiral immersed in a Kapton slab. In particular, the heat is only generated in the Nickel spiral while the Kapton slab is thermally inert. The FVM and DOM are similar to the ones used in [18] for the modeling of the hot-ring method. Thus, we only give a brief description of the model and of the resolution method in this paper and invite the reader to consult [18] for more details.

2.2.1. Governing equations

2.2.1.1. Energy equation in the surrounding medium. The heat balance in a homogeneous semi-transparent, conductive but non convective medium is governed by the energy equation which takes into account the conductive and radiative heat transfer:

$$\rho.C\frac{\partial T(r,z)}{\partial t} = -\vec{\nabla}.\vec{q}_t = -(\vec{\nabla}.\vec{q}_c + \vec{\nabla}.\vec{q}_r) = k\frac{\partial^2 T(r,z)}{\partial r^2} + \frac{1}{r}k\frac{\partial T(r,z)}{\partial r} + k\frac{\partial^2 T(r,z)}{\partial z^2} - \vec{\nabla}.\vec{q}_r \quad (5)$$

2.2.1.2. Energy equation in the hot-disk probe. The probe is opaque and thus, only the conductive heat flux divergence has to be considered. Moreover, the probe is actually made of a Nickel spiral, in which the heat is generated, covered on both sides with Kapton. As mentioned before, heat generation only occurs in the Nickel spiral in which Joule effects take place. Therefore, the energy equation in the Nickel nodes is:

$$\rho_{Ni}.C_{Ni}\frac{\partial T_p(r,z)}{\partial t} = -\vec{\nabla}.\vec{q}_c + \dot{Q} = k_{Ni}\frac{\partial^2 T_p(r,z)}{\partial r^2} + \frac{1}{r}k_{Ni}\frac{\partial T_p(r,z)}{\partial r} + k_{Ni}\frac{\partial^2 T_p(r,z)}{\partial z^2} + \dot{Q} \quad (6)$$

Where

$$\dot{Q} = \frac{Q}{V_{Ni}}$$

While for the nodes made of Kapton:

$$\rho_{Ka}.C_{Ka}\frac{\partial T_p(r,z)}{\partial t} = -\vec{\nabla}.\vec{q}_c = k_{Ka}\frac{\partial^2 T_p(r,z)}{\partial r^2} + \frac{1}{r}k_{Ka}\frac{\partial T_p(r,z)}{\partial r} + k_{Ka}\frac{\partial^2 T_p(r,z)}{\partial z^2} \quad (7)$$

Note that, in our model, the inhomogeneous distribution of the heat generation inside the probe is taken into account, contrary to the quadripole model developed in [15] which assumed that heat is homogeneously generated. Moreover, real thermophysical properties of the constituents of the probe can be taken into account in our model while [15] assumed that the probe is entirely made of Kapton.

2.2.1.3. Radiative transfer equation in the surrounding medium. Regarding the radiative heat transfer, the radiative flux is related to the intensity field in the medium:

$$\vec{q}_r = q_r^r\vec{e}_r + q_r^z\vec{e}_z \text{ with } q_r^r(r,z) = \int_{\Omega=4\pi} I(r,z,\theta,\varphi)\mu.d\mu; q_r^z(r,z) = \int_{\Omega=4\pi} I(r,z,\theta,\varphi)\xi.d\xi \quad (8)$$

and

$$\vec{\nabla}.\vec{q}_r = \frac{1}{r}\frac{\partial}{\partial r}(rq_r^r) + \frac{\partial q_r^z}{\partial z} \quad (9)$$

The radiation intensity field is governed by the Radiative Transfer Equation (RTE) described in details in [18]. For a 2-D axisymmetric radiative transfer in an homogeneous and isotropic semi-transparent material with azimuthal symmetry, this equation is:

$$\frac{\mu}{r}\frac{\partial(r.I(r,z,\theta,\varphi))}{\partial r} - \frac{1}{r}\frac{\partial(\eta.I(r,z,\theta,\varphi))}{\partial\varphi} + \xi\frac{\partial I(r,z,\theta,\varphi)}{\partial z} + \beta.I(r,z,\theta,\varphi) = \kappa.I^0(T) + \frac{\sigma}{4\pi}\int_{\Omega'=4\pi} P(\theta').I(r,z,\theta',\varphi')d\Omega' \quad (10)$$

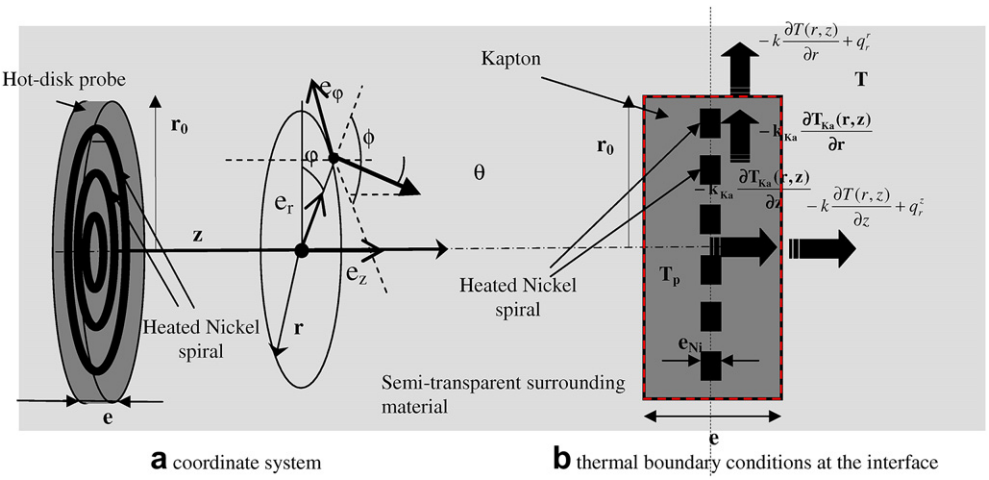

Fig. 1. Illustration of the composition of the probe and the thermal boundary conditions around the probe.

We can notice that it is necessary to know the temperature field in the medium to solve the RTE and to determine the radiation intensity field.

2.2.1.4. Radiative boundary conditions. The boundary conditions at the interface between the surrounding medium and the disk probe are related to the emissivity of the probe (Kapton) and temperature at the surface of the probe:

$$\begin{aligned} I(r_0,z,\theta,\varphi) &= \varepsilon_{Ka} I^0(T_p(r_0,e/2)) + \frac{1-\varepsilon_{Ka}}{\pi} \int_{\Omega'=2\pi;\mu'<0} I(r_0,z,\theta',\varphi').|\mu'|d\Omega \quad \text{for } \mu > 0 \text{ and } |z| < e/2 \\ I(r,\pm e/2,\theta,\varphi) &= \varepsilon_{Ka} I^0(T_p(r,\pm e/2)) + \frac{1-\varepsilon_{Ka}}{\pi} \int_{\Omega'=2\pi;\xi'<0} I(r,\pm e/2,\theta',\varphi').|\xi'|d\Omega' \quad \text{for } \xi > 0 \text{ and } r < r_0 \end{aligned} \tag{11}$$

We also have the following relations for the radiative intensities far from the disk probe:

$$\begin{aligned} I(r\to\infty,z,\theta,\phi) &= I^0(T_{ext}) \text{ for } \mu < 0 \text{ and } I(r,z\to+\infty,\theta,\varphi) \\ &= I^0(T_{ext}) \text{ for } \xi < 0 \end{aligned} \tag{12}$$

2.2.1.5. Thermal boundary conditions. At the interface between the probe surface (Kapton) and the surrounding material, if we take into account the thermal contact resistance and the radiative heat transfer, the thermal boundary conditions are:

$$\begin{aligned} &-k_{Ka}\left.\frac{\partial T_p(r,z)}{\partial z}\right|_{z=\pm e/2} = -k\left.\frac{\partial T(r,z)}{\partial z}\right|_{z=\pm e/2} + q_r^z|_{z=\pm e/2} \quad \text{for } r<r_0 \\ &T_p(r,\pm e/2) = T(r,\pm e/2) + R_c.\varphi \text{ with } \varphi = -k_{Ka}\left.\frac{\partial T_p(r,z)}{\partial z}\right|_{z=\pm e/2} \end{aligned} \tag{13}$$

$$\begin{aligned} &-k_{Ka}\left.\frac{\partial T_p(r,z)}{\partial r}\right|_{r=r_0} = -k\left.\frac{\partial T(r,z)}{\partial r}\right|_{r=r_0} + q_r^r|_{r=r_0} \quad \text{for } |z|<e/2 \\ &T_p(r_0,z) = T(r_0,z) + R_c.\varphi \text{ with } \varphi = -k_{Ka}\left.\frac{\partial T_p(r,z)}{\partial r}\right|_{r=r_0} \end{aligned} \tag{14}$$

Similarly, at the interface between the Nickel and Kapton parts of the probe, the energy conservation leads to the following thermal boundary conditions:

$$-k_{Ka}\left.\frac{\partial T_p(r,z)}{\partial z}\right|_{z=\pm eNi/2^+} = -k_{Ni}\left.\frac{\partial T_p(r,z)}{\partial z}\right|_{z=\pm eNi/2^-} \quad \text{for } r<r_0 \tag{15}$$

$$-k_{Ka}\left.\frac{\partial T_p(r,z)}{\partial r}\right|_{r^+} = -k_{Ni}\left.\frac{\partial T_p(r,z)}{\partial r}\right|_{r^-} \quad \text{for } |z| < e/2 \tag{16}$$

The other boundary conditions are:

$$\begin{aligned} &T(r,z,t) = T_{ext}; T_p(r,z,t) = T_{ext} \quad \text{For all } r \text{ and } z \text{ when } t \le 0 \\ &T(r,z,t) = T_{ext} \quad \text{For } r\to\infty \text{ or } z\to\infty \end{aligned} \tag{17}$$

2.2.2. Numerical resolution of the transient coupled heat transfer

In order to solve the energy equations Eqs. (5)–(7) and to calculate numerically the variation of the temperature field in the probe and in the surrounding material during the transient heat transfer, we use an explicit time marching technique. As it is necessary to know the temperature field to solve the RTE and to compute $\vec{\nabla}.\vec{q}_r$ in the surrounding material, an internal iterative process should be performed at each time step to produce consistency between the temperature profile and the radiation field. However, when the time interval between two time steps is small ($\Delta t < 0.1$ s in our study), this internal iterative process is superfluous and the temperature field at the new time step could be calculated directly using the radiation intensity field at the previous time step without causing errors.

2.2.2.1. Resolution of the energy equation and computation of the temperature field. At each time step, the resolution of the energy equations (Eqs. (5)–(7)) permit to compute the new temperature distribution in the surrounding medium and in the probe from the temperature and radiation intensity profiles at the previous time step. To solve these equations we use a spatial discretization dividing the space in $nR \times nZ$ elementary volume. As the plane $z = 0$ is a plane of symmetry, we only consider the heat transfer in the region $z > 0$. In order to limit the computation time and memory requirement, the heat transfer problem is solved in a finite volume around the probe. Then the calculations are restricted to $0 < r < r_{max}$ and $0 < z < z_{max}$. This volume must be sufficiently large to make sure that the theoretical temperature profile inside the disk is not influenced by the value of r_{max} and z_{max}. A node is placed at the center of each elementary volume of coordinate r_i and z_j and the numerical resolution computes the evolution of the temperature (noted $T_{i,j}$) at these nodes. The elementary volumes with $i \le nR_p$ and $j \le nZ_p$ correspond to probe nodes (thermal properties ρ_{Ka}, C_{Ka}, k_{Ka} and ρ_{Ni}, C_{Ni}, k_{Ni}) while the other elements are made of surrounding material (thermal properties ρ, C, k, β, σ, $P(\theta')$).

The spatial discretization along the z-axis is constant in the probe but provides narrower volumes in the surrounding medium near the probe where important temperature gradients are found. Then, we have:

$$\begin{aligned} &\Delta z_j = e/nZ_j \text{ for } j=1, \Delta z_j \\ &= \left[\cos\left(\frac{(j-1)\pi}{2nZ}\right) - \cos\left(\frac{j\pi}{2nZ}\right)\right]\left(z_{max} - \frac{e}{2}\right) \text{ for } j = nZ_p, nz \end{aligned} \tag{18}$$

Similarly, the spatial discretization along the radial coordinate is constant in the probe and provides narrower volumes in the surrounding material near the probe:

$$\text{for } i = 1, nR_p\{0 < r < r_0\}\ ; \Delta r_i = \frac{r_0}{nR_p} \tag{19}$$

$$\begin{aligned} &\text{for } i = nR_p+1, nR; \{r_0 < r < r_{max}\}; \Delta r_{i+1} \\ &= 1.8 \times \Delta R_i \text{ and } \sum_{i=nRp+1}^{nR} \Delta r_i = r_{max} - r_0 \end{aligned} \tag{20}$$

For the nodes containing the semi-transparent surrounding medium, which are not in contact with the disk (nodes (i,j); $i = nR_p + 1$, nR and $j = nZ_p + 1$, nZ), if we express the energy equation Eq. (5) in a discretised form, we obtain:

$$T_{i,j}^{t+1} = T_{i,j}^{t} + \frac{\Delta t}{\rho C}\left[k\frac{\dfrac{T_{i+1,j}^{t}-T_{i,j}^{t}}{\Delta r_{i+1}/2+\Delta r_i/2} - \dfrac{T_{i,j}^{t}-T_{i-1,j}^{t}}{\Delta r_i/2+\Delta r_{i-1}/2}}{\Delta r_i} + \frac{k}{r_i}\frac{T_{i+1,j}^{t}-T_{i-1,j}^{t}}{\Delta r_i+\Delta r_{i-1}/2+\Delta r_{i+1}/2} + k\frac{\dfrac{T_{i,j+1}^{t}-T_{i,j}^{t}}{\Delta z_{j+1}/2+\Delta z_j/2} - \dfrac{T_{i,j}^{t}-T_{i,j-1}^{t}}{\Delta z_j/2+\Delta z_{j-1}/2}}{\Delta z_j} - \left(\vec{\nabla}.\vec{q}_r\right)_{i,j}^{t}\right] \quad (21)$$

where $\left(\vec{\nabla}.\vec{q}_r\right)_{i,j}^{t}$ is the divergence of the radiative heat flux at the node i,j at time step t

For the nodes of surrounding materials placed near the probe a similar discretised relation could be obtained by applying an energy balance.

The temperature of the probe nodes at the new time step are obtained from the energy equation (Eqs. (6) and (7)) and the boundary conditions (Eqs. (13) and (14)) expressed in a discretised forms.

Finally, the other thermal boundary conditions in a discretised form are:

$$T_{i,j}^{0} = T_{ext} \text{ for all } j \text{ and } i; \quad T_{nR+1,j}^{t} = T_{ext} \text{ for all } t \text{ and } j; \quad T_{i,nZ+1}^{t} = T_{ext} \text{ for all } t \text{ and } i \quad (22)$$

At each time step, the mean temperature T_p^t of the disk probe is obtained by simply averaging the temperatures computed in each probe element:

$$T_p^t = \frac{\sum_{i=1}^{nRm}\sum_{j=1}^{nZm} T_{i,j}^{t}.V_{i,j}}{V_p} = \frac{\sum_{i=1}^{nRm}\sum_{j=1}^{nZm} T_{i,j}^{t}.V_{i,j}}{\sum_{i=1}^{nRm}\sum_{j=1}^{nZm} V_{i,j}} \quad (23)$$

2.2.2.2. Resolution of the 2-D axisymmetric RTE using the discrete ordinates method. In order to calculate the radiative flux $(q_r^r)_{i,j}$ and $(q_r^z)_{i,j}$ and the radiative flux divergence $\left(\vec{\nabla}.\vec{q}_r\right)_{i,j}$ in each point of the spatial discretization of the surrounding material, it is necessary to solve the 2-D axisymmetric Radiative Transfer Equation (Eq. (10)). Several numerical methods can be used to solve the RTE (spherical harmonics method, the zone method of HOTTEL, the ray-tracing methods …). In our study, we use the Discrete Ordinates Method based on a spatial discretization of the area around the circular probe and on an angular discretization of the space. The angular discretization allows replacing the angular integrals by finite summations over n_d discrete directions m (μ_m, η_m, ξ_m) with given weighting factors w_m. For convenience purpose, the spatial discretization is the same as the one used for the numerical resolution of the energy equation. The 2-D discrete ordinates solution for a radiatively participating medium in a cylindrical enclosure has been widely described, notably by Carlson and Lathrop [19] or Jendoubi et al. [20] and we will not detail it in this article.

Once the discretised intensity field in the semi-transparent medium around the circular probe has been determined, the radiative flux and radiative flux divergence are calculated using the discretised form of Eq. (8):

$$(q_r^r)_{i,j} = \left[\sum_{m=1}^{nd} I_{i,j}^{m}\mu_m w_m\right] \text{ and } (q_r^z)_{i,j} = \left[\sum_{m=1}^{nd} I_{i,j}^{m}\xi_m w_m\right] \quad (24)$$

$$\left(\vec{\nabla}.\vec{q}_r\right)_{i,j} = \frac{1}{r_i}\frac{r_{i+1/2}(q_r^r)_{i+1/2,j} - r_{i-1/2}(q_r^r)_{i-1/2,j}}{\Delta r_i} + \frac{(q_r^z)_{i,j+1/2} - (q_r^z)_{i,j-1/2}}{\Delta z} \quad (25)$$

2.2.3. Validation of the numerical model

The numerical resolution of the 2-D axisymmetric radiative problem has been tested by comparing the results of our model with various published results [20,21] for different media where only radiative transfer occurs and for different radiative boundary conditions. The accuracy of the numerical method is strongly dependent on the quadrature used for the angular discretization. We have tested different S_N quadratures. The results obtained when using the quadrature points and weights of the S_6 scheme prove to be quite satisfactory in all cases and we will use this quadrature in all the following numerical calculations.

Concerning the entire 2-D transient radiation/conduction coupling problem, few previous results have already been published [22,23]. We have compared the results of our numerical model with these studies and found a good agreement. However, the results presented in these papers concern theoretical problems with boundary conditions notably different from the ones encountered in our hot-disk simulation. Thus, it seems to us that it is more suitable to illustrate the validity of our numerical resolution by comparing with TPS results available for two ideal cases:

- Infinite purely conductive medium ($\beta \to \infty$, $k = 0.035$ Wm^{-1} K^{-1}, $\rho.C = 35 \times 1200$ J/m^3/K) surrounding a thermally neutral hot-disk probe without thermal contact resistance
- Infinite transparent medium ($\beta = 0$; $k = 0.035$ Wm^{-1} K^{-1}, $\rho.C = 35 \times 1200$ J/m^3/K) surrounding a thermally neutral hot-disk probe without thermal contact resistance

Although these two ideal cases are limiting, they seem to us more appropriate to illustrate the validations of the model as the boundary conditions are close to the real problem.

The first ideal test case corresponds to the classical TPS method used in the hot disk thermal constants analyzer (HD) manufactured by hot disk AB. The variation of the temperature of the disk is then given by Eq. (1). In order to model numerically this case, the computations were carried out by setting $\rho_{Ni}.C_{Ni} = \rho_{Ka}.C_{Ka} = \rho.C = 100 \times 1200 J/m^3.K$, $k_{Ni} = k_{Ka} = k = 0.035 W/m/K$ (no thermal inertia of the probe), $R_c = 0$ (no thermal contact resistance) and $(q_r^r)_{i,j} = 0$, $(q_r^z)_{i,j} = 0$ and $\left(\vec{\nabla}.\vec{q}_r\right)_{i,j} = 0$ (purely conductive medium) and by applying an homogeneous heat generation in the entire probe.

We compared, on Fig. 2, the results of the analytical formula for an homogeneously heated probe ($n \to \infty$:Eq. (3)) with the temperature rise predicted by our numerical simulation using the following parameters $r_0 = 0.003189$ m, $e = 60$ μm, $Q = 0.01$ W, $T_{ext} = 296$ K. For both calculations, we set the numerical parameter $nR_p = 8$, $nR = 22$, $nZ = 33$, $r_{max} = 0.2$ m and $z_{max} = 0.1$ m. We have checked that these values of r_{max} and z_{max} are sufficiently important in order for the numerical results to remain independent of their values. In the next, all the numerical computations have been conducted with the preceding values of nR_p, nR, nZ, r_{max} and z_{max}. On Fig. 2, we have also depicted the evolutions of the discrepancies $(\Delta T^*(t) = |\Delta T_{p,ana}(t) - \Delta T_{p,num.}(t)|/\Delta T_{p,ana}(t))$.

The comparison between analytical and numerical results show that the temperature rise computed by neglecting radiative heat flux divergence is very close to the analytical solution as the relative differences are always lower than 0.5% when $t > 5$ s. We notice that the maximum differences between analytical and numerical results are found for the very low values of time t.

Regarding the second test case, it corresponds to the transparency limit $\beta = 0$. Under this assumption, the conductive and radiative contributions can be evaluated separately as the surrounding medium does not participate to the radiative transfer

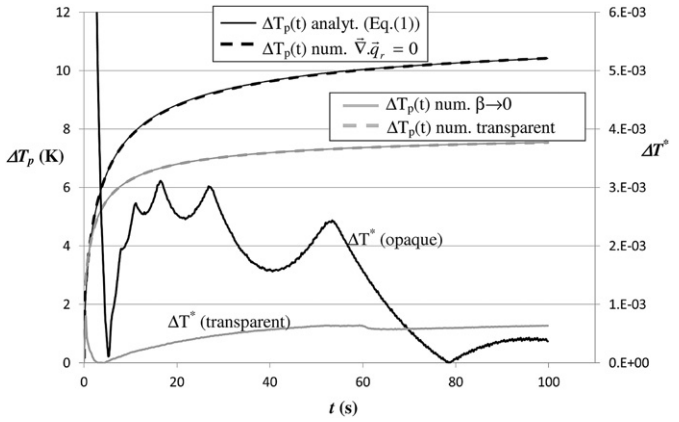

Fig. 2. Comparison of the thermograms obtained analytically and numerically for the two ideal cases used for the validation (opaque and transparent).

$((\vec{\nabla}.\vec{q}_r)_{i,j} = 0)$. There is a direct radiative exchange between the probe and the surrounding environment at $T = T_{ext}$. Therefore, the radiative heat flux emitted by the probe only depends on its emissivity and its local temperature. It can be evaluated by the analytical relation:

$$q^z_{r_{i\le nRm, j=nZm+1/2}} = \varepsilon_p \sigma_{SB}\left(T^4_{i,j=nZm} - T^4_{ext}\right) \quad \text{and} \quad q^r_{r_{nRm\pm1/2, j\le nZm}} = \varepsilon_p \sigma_{SB}\left(T^4_{nRm,j\le nZm} - T^4_{ext}\right) \tag{26}$$

The numerical results obtained by setting $(\vec{\nabla}.\vec{q}_r)^t_{i,j} = 0$ and using the previous boundary conditions Eq. (22) with $\varepsilon_p = 1$ in the purely conductive problem have been compared to those obtained by setting $\beta = 10^{-6}$ m^{-1} in the numerical resolution of the conduction–radiation coupling. The deviation between the two numerical methods is always lower than 0.1% in the time range 0–100 s. Thus, the numerical resolution of the radiative problem proves to give satisfactory results.

As a conclusion the calculations carried out for the two limiting cases show that, when using the spatial discretization $nR_m = 8$, $nR = 22$, $nZ = 33$ and the S_6 angular quadrature, our numerical method accurately simulates the temperature rise of the hot disk and near the hot disk probe.

2.3. Identification of thermal properties from hot-disk experiment

Following the principle of hot disk thermal constants analyzer, we have developed an identification procedure to estimate the thermal conductivity and thermal diffusivity from the TPS thermograms. The identification procedure developed is based on a least square fit method which minimizes the difference between the measured temperature $T_{p,exp.}(t)$ of the probe and the temperature $T_{p,th.}(t)$ predicted by the analytical model. The principle is to minimize the function F representing the sum of the quadratic discrepancies between the experimental and theoretical variations of the temperature:

$$F = \sum_{n=1}^{N}\left[\Delta T_{p,\exp}(t_n) - \Delta T_{p,th}(t_n)\right]^2 \tag{27}$$

The evolution of the temperature calculated by the analytical model is influenced by r_0, $\rho.C$, k, $\dot{Q}$, A and t_c. Given that r_0 and Q are known, $\Delta T_{p,th.}(t)$ and F only depend on the 4 parameters $P_1 = k$, $P_2 = \rho.C$, $P_3 = A$ and $P_4 = t_c$ which have to be identified by minimizing F. We have:

$$F = F(\rho.C, k, t_c) = \sum_{n=1}^{N}\left[\Delta T_{p,\exp}(t_n) - \Delta T_{p,th}(t_n)\right]^2 \tag{28}$$

In order to minimize F, the parameters P_k should satisfy the relations:

$$\frac{\partial F}{\partial P_k} = \frac{\partial}{\partial P_k}\left[\sum_{n=1}^{N}\left(\Delta T_{p,\exp}(t_n) - \Delta T_{p,th}(t_n)\right)^2\right] = 0 \Rightarrow \sum_{n=1}^{N}\left[\left(\Delta T_{p,\exp}(t_n) - \Delta T_{p,th}(t_n)\right).\frac{\partial T_{p,num}(t_n)}{\partial P_k}\right] = 0 \quad \text{for } k = 1,4 \tag{29}$$

The partial derivatives $\partial T_{p,num.}(t_n)/\partial P_k$ are called the sensitivity coefficients and represent the rate of variation of the mean temperature of the probe at the time t_n due to a variation of the parameter P_k.

In order to solve this system of non-linear equations, we use the iterative method of Gauss starting from initial values P^0_k. At each iteration level l, the following system of equations is solved:

$$\sum_{n=1}^{N}\left[\left(\Delta T_{p,\exp}(t_n) - \left(\Delta T_{p,th}(t_n)\right)^l\right).\left(\frac{\partial T_{p,th}(t_n)}{\partial P_k}\right)^l\right] = 0 \text{ for } k = 1,4 \tag{30}$$

Moreover, the value $(\Delta T_{p,th.}(t_n))^l$ at the iteration level l can be approximated from the values at the iteration level $l-1$ by the following relation:

$$\Delta T_{p,th.}\left(t_n, [P_k]^l_{k=1,4}\right) = \Delta T_{p,th.}\left(t_n, [P_k]^{l-1}_{k=1,4}\right) + \sum_{k=1}^{N}\left(\frac{\partial T_{p,th}(t_n)}{\partial P_k}\right)^{l-1}.\Delta P^{l-1}_k \tag{31}$$

We finally have to solve the following matrix system, where the superscript l refers to the entire matrixes:

$$\left[A_{k,j}\right]^l.[\Delta P_j]^l = [B_k]^l \tag{32}$$

with

$$A^l_{k,j} = \sum_{n=1}^{N}\left(\frac{\partial T_{p,th.}(t_n)}{\partial P_k}\right)^l.\left(\frac{\partial T_{p,th.}(t_n)}{\partial P_j}\right)^l ; B^l_k = \sum_{n=1}^{N}\left(\left(\Delta T_{p,\exp}(t_n) - \Delta T_{p,th.}(t_n)\right).\frac{\partial T_{p,th.}(t_n)}{\partial P_k}\right)^l$$

This system is solved successively for each iteration level l to calculate the values $[P^{l+1}_k = P^l_k + \Delta P^l_k]_{k=1,4}$ until the ratios $[\Delta P^l_k/P^l_k]_{k=1,4}$ are lower than a convergence criterion.

3. Numerical analysis

The numerical model presented in Section 2.2 has been used to simulate the variations of the temperature $T_p(t)$ for various non-ideal cases for which the radiative heat transfer in the medium and the thermal inertia of the probe are significant. Moreover, in order to produce even more realistic thermograms, the evolutions of the temperature of the probe generated numerically have been noised. This noise consists in the addition of a random artefact to the thermogram, corresponding to a certain proportion No of the maximum temperature:

$$\Delta T'_{p,G}(t_n) = \Delta T_{p,G}(t_n) + (0.5 - \varsigma_n) \times \mathrm{No} \quad \text{for } n = 1, N \qquad (33)$$

Where ζ_n are randomly generated numbers comprised between 0 and 1

Thereafter, the identification procedure described in Section 2.3 has been applied to the numerically generated noised thermograms which are supposed to reproduce realistic experimental thermograms. This has been done by setting $\Delta T_{p,\exp}(t_n) = \Delta T'_{p,G}(t_n)$ in Section 2.3. It is also important to notice that the time intervals $[t_1, t_N]$ used for the identifications correspond to the interval $[t_{\min}, t_{\max}]$ recommended by the manufacturer of the hot disk thermal constants analyzer. Therefore, the difference between the identified and initial thermal conductivity k and thermal inertia $\rho.C$ allows to quantify the errors on the estimations of these properties due to deviations from the ideal experimental conditions of the classical hot-disk method.

N.B: The influence of the thermal contact resistance between the probe and the surrounding medium has also been analyzed. The numerical results show that this resistance has a very slight influence on the temperature rise except for extremely large and unrealistic values of R_c (>1 m^2 K/W). Moreover, compared to the ideal model, it leads to a constant shift of the temperature as previously mentioned by numerous previous studies (Gustavsson and Gustafsson [17] or Jannot and Acem [15]). This constant shift is well-fitted by the constant temperature jump (parameter A) and does not influence the values of the thermophysical parameters k and ($\rho.C$) identified.

3.1. Errors due to the contribution of radiative heat transfer

For materials with low-density having a semi-transparent radiative behavior, radiative heat transfer may be significant, even at ambient temperatures. It is notably the case of low density thermal insulators such as glass and rock wools ([24]) or polymer foams [25]. For such materials, the property of interest is the so-called "equivalent thermal conductivity" characterizing the magnitude of the total heat transfer by conduction and by thermal radiation. In practice, this property has to be evaluated experimentally using the classical guarded hot-plate method. This equivalent conductivity could theoretically not be measured by transient measuring methods (FLASH method, hot-wire method) and noticeably by the hot-disk method since they are all based on the assumption of purely conductive heat transfer. Indeed, the radiative heat transfer obeys mechanisms which are quite different from thermal conduction. However, some specific studies have shown that, under certain conditions, the equivalent conductivity of low-density thermal insulators could be estimated with a satisfying accuracy using the classical FLASH method [4] or the hot-wire method [18].

Therefore, in this section, we have evaluated the possibility to use the hot-disk method to estimate satisfactorily the equivalent conductivity and diffusivity of such materials. We have numerically generated noised thermograms obtained by solving the transient coupled heat transfer (Section 2.). In this section, in order to analyze the only influence of radiative transfer, the thermal contact was neglected and the probe was considered to be thermally neutral: $R_c = 0$ m^2 K/W, $\rho_{Ka}.C_{Ka} = \rho_{Ni}.C_{Ni} = \rho.C$ and $k_{Ka} = k_{Ni} = k$. The dimensions of the probe are: $r_0 = 0.003189$ m, $e = 30$ μm while Kapton is considered as a perfect emitter ($\varepsilon_{Ka} = 1$). For simplicity purpose, we considered that the probes are made of a very important number of concentric rings ($n \to \infty$) so that energy dissipated in the Nickel could be assumed uniformly distributed along the probe radius ($\dot{Q} = C^{st}$ for $|z| \langle \frac{e_{Ni}}{2}$, $R < r_0$) keeping $\dot{Q} = 0$ for $e_{Ni}/2 < |z| < \frac{e}{2}$, $R < r_0$. Then, Eq. (3) can be used to compute $T_{p,th}$ during the identification procedure described in Section 2.3.

The thermo-physical properties of the materials modeled have been chosen in order to be representative of real low-density thermal insulators such as Polyvinyl-chloride foam (Mat. A:PVC) and extruded PolyStyrene foams (Mat. B:XPS).

- for material A.: $\rho = 55$ kg/m^3, $C = 1200$ J/kg/K, $k_{eff} = 0.03$ W/m/K
- for material B.: $\rho = 35$ kg/m^3, $C = 1200$ J/kg/K, $k_{eff} = 0.03$ W/m/K

where k_{eff} is the effective thermal conductivity representing the contribution of conduction alone (through solid and fluid)

The radiative properties used for these materials have been obtained from Ref. [4]. In this study, the authors assumed that the scattering phase functions follow the Henhey–Greenstein law ($P_\lambda(\theta) = 1 - g_\lambda^2/(1 + g_\lambda^2 - 2.g_\lambda.\cos\theta)^{1.5}$). Therefore, they managed to identify the three spectral properties β_λ, ω_λ, and $P_\lambda(\theta)$ using the directional and hemispherical transmittances and reflectances measured on thin and thick slices of foams. The thicknesses of the thin slices were 1.0 mm and 0.87 mm for Mat A. and B. respectively. We depict on the same figure (Fig. 3), the variations of the weighted spectral extinction coefficient $\beta^*_\lambda = \kappa_\lambda + \sigma_\lambda \times (1 - g_\lambda)$ identified for these two materials and the error bars associated with the corresponding uncertainties.

Using the values of β_λ, ω_λ, and $P_\lambda(\theta)$ identified, it is possible to compute the equivalent thermal conductivities $k_{equ,num}$ of the two materials by solving the steady-state 1-D coupled heat transfer between two infinite and perfectly emissive plates maintained at fixed temperatures. This actually corresponds to a numerical simulation of the guarded hot-plate measurement. For this calculation, the numerical model described in [26] has been used. For consistency purpose, we assumed that the plates are, like the probe, perfectly emissive $\varepsilon_h = \varepsilon_c = \varepsilon_p = 1$. $k_{equ,num}$ may also depend on the space interval L between the plates. However, we have checked that these variations are almost negligible when L exceeds a relatively low value. Therefore, for common slab thicknesses (>50 mm), the equivalent conductivity could be considered independent of L.

The value of $k_{equ,num}$ depends on the mean temperature of the hot and cold plates since the radiation intensity emitted is proportional to T^4 but is almost independent of the temperature difference between them. In order to analyze the influence of the

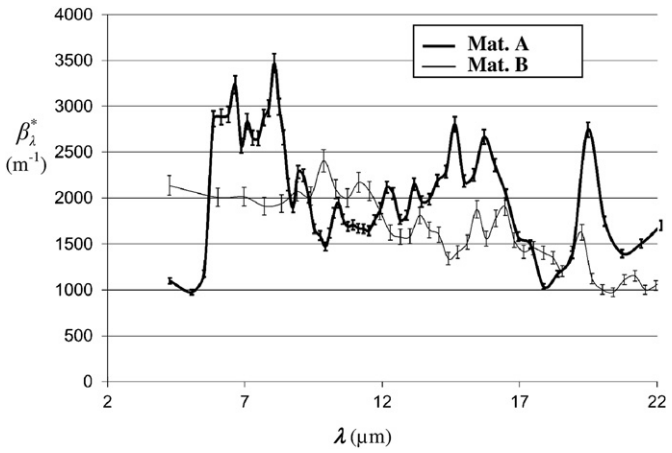

Fig. 3. Spectral variations of the scaled extinction coefficient of materials A and B (identified from spectrometric measurements in Ref. [4]).

temperature on the hot-disk measurement, we conducted the identification of k and $(\rho.C)$ using two different heating powers $Q = 0.02$ W and 0.005 W.

The values of thermal properties identified as well as the relative deviations from the real values $(\Delta k = |k_{ident.} - k|/k; \Delta(\rho.C) = |(\rho.C)_{ident} - (\rho.C)|/(\rho.C))$ are summarized in Table 1 where we also indicate the mean discrepancies between numerically generated and identified thermograms $(\langle \Delta T^* \rangle = \sum_{t=t\min}^{t=t\max}(|\Delta T'_{p,G.}(t) - \Delta T_{p,th.}(t)|)/\sum_{t=t\min}^{t=t\max}\Delta T'_{p,G.}(t))$. We also have compared the numerically generated and identified thermograms as well as the evolutions of the discrepancies $(\Delta T^*(t) = \Delta T'_{p,G}(t) - \Delta T_{p,th.}(t)/\Delta T'_{p,G}(t))$ on Figs. 4 and 5.

The values of $k_{equ,num}$ indicated in Table 1 have been computed for a temperature corresponding to the mean temperature of the probe in the time interval used for the identification.

The results obtained clearly indicate that, for low-density polymer foams, the presence of a radiative transfer contribution does not impact the accuracy of the hot-disk method. The thermal conductivity estimated by this method actually corresponds to the equivalent conductivity. Indeed, one can remark that the relative errors on k compared to k_{equ} is very low (<3%) in every cases considered. The errors on $(\rho.C)$ are more important and can reach approximately 4–5% for sample B in which the radiative contribution is the most important. However, this remains acceptable. One can also notice on Figs. 4 and 5 that the fitting between numerically generated and identified thermograms is excellent. The relative deviations ΔT observed are almost entirely due to the noise added to the generated thermograms. It is also interesting to notice that the conductivities identified are sensitive to the level of temperature reached during the measurement since the values for a heating power $Q = 0.02$ W are slightly more important than for $Q = 0.005$ W. This illustrates the fact that the radiative heat transfer contribution increases rapidly with the temperature leading to an increase of the equivalent conductivity.

However, it should be reminded that these conclusions have been obtained assuming that the thermal contact resistance and thermal properties (inertia and conductivity) of the probe do not disturb the measurement. We will verify this latter assumption in the following section.

3.2. Errors due to the thermal properties of the probe

Another source of error in the estimation of the thermal properties using the hot-disk technique might be caused by the fact that the thermal inertia and conductivity of the probe are different from the ones of the material tested. Indeed, insulating materials have the particularity to exhibit, at the same time, low thermal inertia and thermal conductivities. We have evaluated the importance of this source of errors by conducting the identification on thermograms generated numerically using realistic values of the dimensions, composition and thermal properties of the probe which are commonly encountered. We used: $r_0 = 0.03189$ m, $e = 30$ μm, $e_{Ni} = 0.5 \times e = 15$ μm, $\rho_{Ka} = 1420$ kg/m^3, $C_{Ka} = 1090$ J/(kg K), $k_{Ka} = 0.2$ W/m/K, $\rho_{Ni} = 8900$ kg/m^3, $C_{Ni} = 440$ J/(kg K), $k_{Ni} = 91$ W/m/K. At the same time, we have also generated numerical thermograms for the case where an "ideal" probe was used, i.e., its thermal properties are identical to that of the material $\rho_{Ka}.C_{Ka} = \rho_{Ni}.C_{Ni} = \rho.C$ and $k_{Ka} = k_{Ni} = k$. The other properties are the same as the "real" probe: $r_0 = 0.03189$ m, $e = 30$ μm, $e_{Ni} = 15$ μm. The identification procedure has also been conducted on these thermograms.

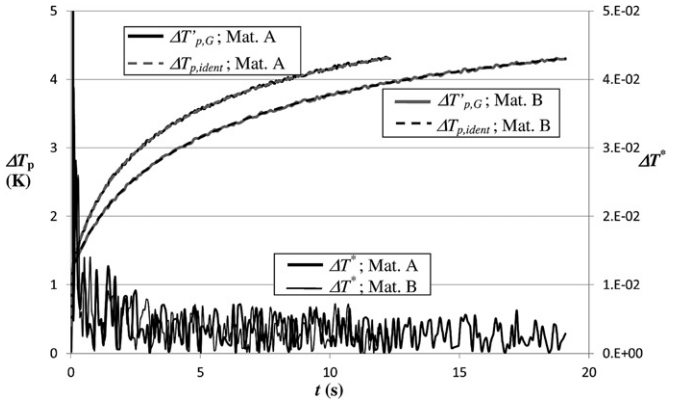

Fig. 4. Comparison of the generated and identified thermograms for semi-transparent Materials A and B using ideal probes with $Q = 0.005$ W.

Like in previous section, we considered that the probes are made of a very important number of concentric rings $(n \to \infty)$ so that energy dissipated in the Nickel could be assumed uniformly distributed along the probe radius.

The computations were conducted for two purely conductive material with thermal inertia and conductivities representative of classical low-density thermal insulators:

- Material 1: A typical PS foam with $k = 0.035$ W/m/K, $\rho = 35$ kg/m^3, $C = 1200$ J/(kgK).
- Material 2: A typical superinsulating Silica aerogel with $k = 0.02$ W/m/K, $\rho = 150$ kg/m^3, $C = 1200$ J/(kgK)

We do not consider deliberately the radiative heat transfer in the materials although it may contribute noticeably to the heat transfer (especially for PS foams). Actually, we assume that the materials are purely conductive with an equivalent conductivity encompassing the conductive and radiative contributions in order to analyze the only influence of the thermal properties of the probe on the results of the identification. The other parameters used for the numerical generation of the noised thermograms are: $Q = 0.02$ (Mat. 1) and 0.005 W (Mat. 1), $T_{init} = 296$ K, $\zeta = 1\%$ and $R_c = 0$ K/(m^2 W).

The results of the identifications are summarized on Table 2 and the comparisons of the identified and generated thermograms are depicted on Figs. 6 and 7 (Table 3).

As expected, the relative errors obtained when considering an "ideal" probe ($\rho_{Ka}.C_{Ka} = \rho_{Ni}.C_{Ni} = \rho.C$ and $k_{Ka} = k_{Ni} = k$) are quite negligible for the two properties identified and for both materials. One can also notice the very good fitting ($\langle \Delta T^* \rangle = 3.6 \times 10^{-3}$ and 3.3×10^{-3}) and the very low values of parameter A (0.0165 and

Table 1
Results of the identification procedure for thermograms generated for semi-transparent polymer foams using an ideal probe.

Mat.	Q (W)	k_{ident} W/m/K	$k_{equ,num}$ W/m/K	Δk (%)	$(\rho.C)_{ident}$ (J/m^3)	$\Delta(\rho.C)$ (%)	A_{ident} (K)	$(t_c)_{ident}$ (s)	$\langle \Delta T^* \rangle$
A	0.02	0.0362	0.0373	3.0	65091	1.4	0.359	0.069	0.0039
	0.005	0.0362	0.0366	1.3	67423	2.1	0.133	0.0391	0.0034
B	0.02	0.0361	0.0359	0.5	39984	4.8	0.211	0.059	0.0038
	0.005	0.0363	0.0353	2.8	43620	3.8	0.162	0.0128	0.0034

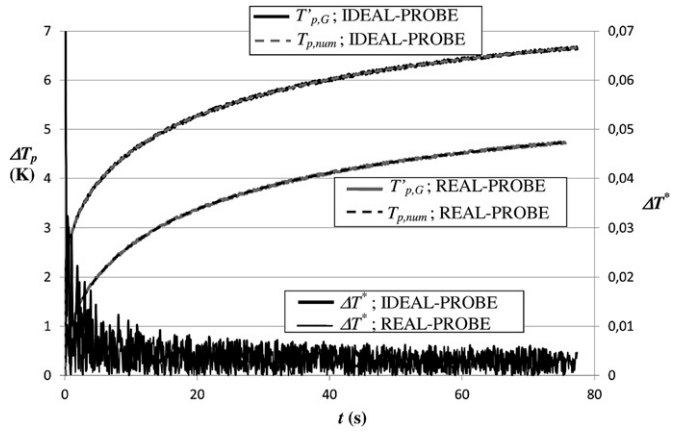

Fig. 5. Comparison of the generated and identified thermograms for semi-transparent Materials A and B using ideal probes with Q = 0.02 W.

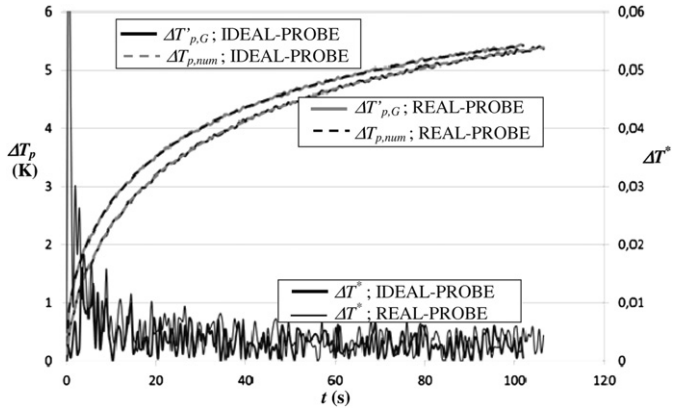

Fig. 6. Comparison of the generated and identified thermograms for Material 1 using ideal and real probes.

0.085 K) and t_c (-4.7×10^{-5} and -0.026 s) indicating that the corrections of the thermograms from the ideal case are very slight.

On the other hand, the results for the thermograms obtained with the real probe show that, the fact that thermal properties of the probes differ from the ones of the material tested, influences noticeably the accuracy of the hot-disk measurement. Both the thermal inertia ($\rho_{Ka}.C_{Ka}$) ($\rho_{Ni}.C_{Ni}$) and thermal conductivities k_{Ka} and k_{Ni} of the probe disturbs the ideal measurement. Indeed, Materials1 and 2 have thermal inertia noticeably lower than that of the probe materials (Ni, Ka), and thus the temperature rise of the probe are later than when an ideal probe is considered. The energy required to heat the real probe is then noticeably more important and needs a larger heating time so that the thermogram is delayed. The fitting procedure well reproduce this delay ($\Delta T^* = 5.7 \times 10^{-3}$ and 3.8×10^{-3}) by identifying values of A and t_c which are no more negligible: $A = -2.94$ K; $t_c = 0.296$ s for material 1 and $A = -1.22$ K; $t_c = 0.27$ s for material 2. However, one can notice that the errors on the thermal properties identified are not negligible especially for Material 1 for which it reaches 11.7% and 47% for k and $\rho.C$ respectively. The errors for Material 2 are noticeably lower (4.0% for k and 0.3% for $\rho.C$) and remain acceptable if a relative error of 5% is tolerated.

The fact that the errors are lower for Material 2 than Material 1 can be explained by the lower difference between its thermal inertia ($\rho.C = 1.8 \times 10^{-5}$ J/m^3/K for Material 1 and $\rho.C = 4.2 \times 10^{-4}$ J/m^3/K for Material 2) and the inertia of the constituents of the probe ($\rho_{Ka}.C_{Ka} = 1.55 \times 10^6$ J/m^3/K; $\rho_{Ni}.C_{Ni} = 3.92 \times 10^6$ J/m^3/K). Therefore, the disturbance of the thermogram due to the inertia of the probe (delay of the temperature rise) is so important for sample $n°1$ that it cannot be reproduced satisfactorily by the artificial fitting parameters A and t_c. On the other hand, the delay of the temperature rise for sample 2 can be matched more accurately by A and t_c keeping acceptable values for the thermal properties k and ($\rho.C$) identified. As a conclusion, it appears that when the difference between the thermal inertia of the probe and of the material tested exceeds one order of magnitude, the thermal properties given by the classical the Hot-disk method must be questioned.

4. Experimental validation

The preceding sections have permitted to highlight some of the limitations of the classical hot-disk method when applied to thermal insulators. However, these conclusions as well as the order of magnitude of the errors caused by the deviations from the ideal case are only based on a numerical study. In order to validate these theoretical conclusions, we have conducted an experimental study on standards thermal insulators in which radiative heat transfer is non-negligible. Two different materials have been considered: an XPS foam and a superinsulating Silica aerogel. The thermal properties of the XPS foam sample have been characterized accurately by steady-state techniques at $T = 296$ K:$k_{equ} = 0.035$ W/m/K, $\rho = 33.0$ kg/m^3, $C = 1270$ J/kg/K, ($\rho.C$) = 41910 J/(m^3 K). The Silica aerogel sample, denominated *Spaceloft*, is produced by the Aspen Aerogels® Company. The properties given by the manufacturer are: $k_{equ} = 0.0162$ W/m/K; $\rho = 150$ kg/m^3; $C = 1100$ J/(kg K); ($\rho.C$) = 1,65,000 J/(m^3 K).

It has been proven in Section 3, that the application of the hot-disk method to low-density insulating materials is questionable due to the low thermal conductivity and low thermal inertia of these materials when compared to the thermal properties of the probe. The hot-disk probe used has the following characteristics: $r_0 = 3.189$ mm, $n = 7$, $e \approx 25$ μm. The measurements were conducted by sandwiching the hot-disk probe between two slabs of XPS foam sample with 80 mm in thickness or Silica aerogel with 8 mm in thickness. It can be easily checked that these thicknesses are significantly more important than the distance $D \approx 2.\sqrt{(a.t)}$ traveled by the heating at the end of the measurement and thus that no "side effect" occurs for both measurement. A mechanical load has been applied to the sandwich in order to minimize the thermal contact resistance at the interface between the probe and the samples.

We have applied the identification procedure used in Section 3 to the thermograms obtained at a temperature of 296 K. Since the number of concentric rings of the experimental device is, here, finite, we used Eq. (1) with $n = 7$ rather than Eq. (3) for the direct model. The measured thermograms used for the validation are

Table 2
Results of the identification procedure for thermograms generated with real and ideal probes on the three materials considered.

Material	Probe	k_{ident} (W/m/K)	Δk (%)	$(\rho.C)_{ident}$ (J/m^3/K)	$\Delta(\rho.C)$ (%)	A_{ident} (K)	$(t_c)_{ident}$ (s)	$\langle \Delta T^* \rangle$
Mat. 1	IDEAL	0.0349	0.14	41491	1.2	0.0165	-5×10^{-5}	0.0036
	REAL	0.0309	**11.7**	61853	**47.3**	−2.94	−0.296	0.0057
Mat. 2	IDEAL	0.0199	0.45	1.81E5	0.67	0.085	−0.026	0.0033
	REAL	0.0192	4.0	1.79E5	0.3	−1.218	0.27	0.0038

Bold value signify that the error values are greater than 5%.

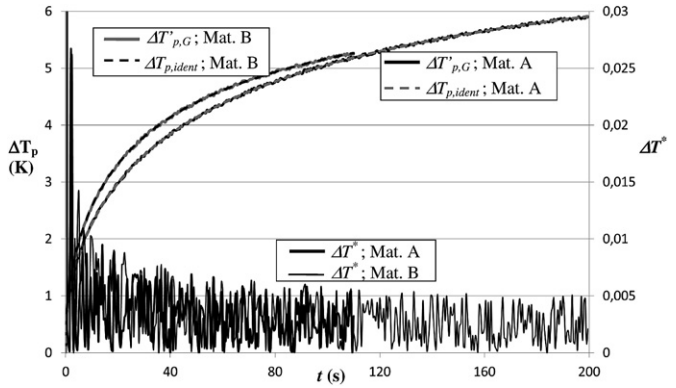

Fig. 7. Comparison of the generated and identified thermograms for Material 2 using ideal and real probes.

Table 3
Results of the identification procedure for thermograms measured on the standard polystyrene foam and the silica aerogel used for validation.

	k_{ident} (W/m/K)	Δk (%)	$(\rho.C)_{ident}$ (J/m^3/K)	$\Delta(\rho.C)$ (%)	A_{ident} (K)	$(t_c)_{ident}$ (s)	$\langle \Delta T \rangle$
XPS foam	0.0365	4.1	55120	**39.2**	−3.05	−0.138	0.0042
Silica aerogel	0.0179	**10.6**	92510	**43.9**	0.434	0.245	0.0012

Bold value signify that the error values are greater than 5%.

actually average thermograms obtained from 5 consecutive measurements on the same sample and under identical conditions.

It is interesting to observe that the fitting between experimental and identified thermograms is very good (Figs. 8 and 9) for the two samples considered. However, the values of the parameters A and t_c identified are significant. This confirms that some strong deviations from the ideal measuring conditions are encountered in both cases. One can also remark that the thermal conductivity identified from the measured thermogram are quite acceptable for both materials (+4.0% for the XPS foam and +10% for the silica aerogel). On the other hand, the thermal inertia identified diverge more noticeably from the real values (+39% for XPS foam and −44% for silica aerogel).

The fact that the thermal conductivity of the XPS foam sample measured by the hot-disk technique is satisfactory could appear inconsistent with the conclusions of Section 3.2 which predicts larger relative errors (>10%) for a similar material (Material 1). However, the error on the value of $(\rho.C)$ are well predicted by the

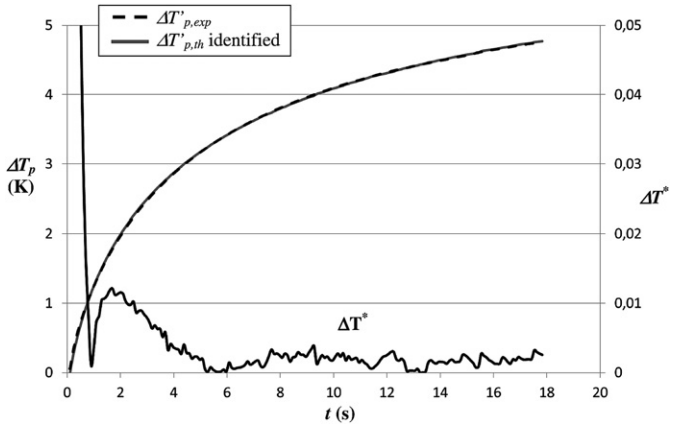

Fig. 8. Comparison of the measured and identified thermograms for the standard polystyrene foam used for validation.

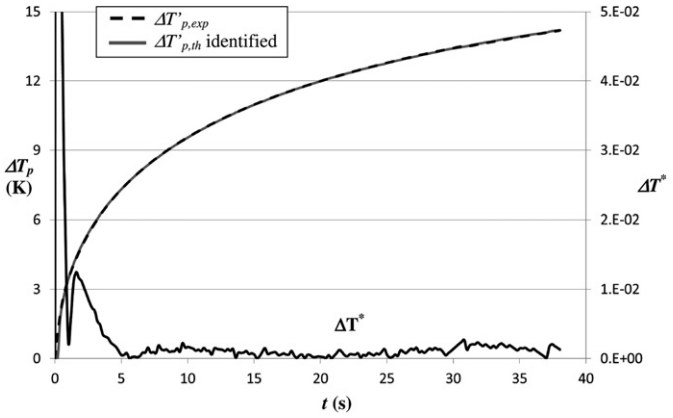

Fig. 9. Comparison of the measured and identified thermograms for the super-insulating silica aerogel used for validation.

numerical results of Section 3.2. Similarly, for the silica aerogel, the significant difference between the identified and real thermal inertia does not fully validate the conclusions of Section 3.2 for Material 2. This might be due to the presence of other parasitical phenomenons such as thermal leaks by the Nickel ring used for the heating. Indeed, these thermal losses might become non-negligible when measurements are conducted on materials with very low conductivities. Anyway, the experimental results confirm that the utilization of the hot-disk technique is questionable for low-density materials, at least for estimating their thermal inertia.

5. Conclusions

Measuring accurately the thermal properties of insulating materials still constitutes a big challenge since it generally requires long measuring times and heavy measurement devices. In light of this, the hot-disk measuring technique (also referred as TPS method) developed during the last two decades presents several strong assets according to the distributor *hot disk AB*:

- the required measurement time is relatively short (few hundreds of seconds at max);
- the probe and measuring equipment are simple and easy to use;
- the size of the samples required is relatively small (few mm in thickness), no specific shape is necessary;
- according to the manufacturer, accurate measurements (<5% for both k and a) can be obtained for a wide range of temperatures (cryogenic up to 1000 K) and a wide range of thermal properties ($0.005 < k < 500$ W/mK; $0.1 > a > 100 \times 10^{-6}$ m^2/s; $(\rho.C)$ up to 5×10^6 J/m^3/K).
- both the thermal conductivity and diffusivity can be measured simultaneously while two measurements are generally required when using other techniques.

Consequently, the hot-disk method is currently largely used with apparent satisfaction for a wide range of materials and temperature. However, the level of accuracy of the method when applied to low-density insulators has not been studied extensively and remains questionable.

In order to meet this challenge, we have developed a numerical model of resolution of the coupled heat transfer problem around real hot-disk probes. This model allows us to simulate numerically the thermal response of the probe for experimental conditions diverging from the ideal conditions assumed in the fitting

procedure (thermally neutral probe, purely conductive heat transfer ….). A least square fit-method associated with an analytical simulation of the purely conductive heat transfer around the probe is applied to the generated thermograms. It allows estimating the errors made on the thermal properties estimated by the classical hot-disk fitting procedure when measurements are conducted on different thermal insulators exhibiting a low thermal inertia (XPS foam, silica aerogel) and/or a significant radiative contribution (XPS foam).

The analysis of the numerical results reveals that the presence of a significant radiative transfer has almost no influence on the accuracy of the measurement. Therefore, the thermal conductivity estimated by the hot-disk method for low-density semi-transparent materials actually corresponds to their equivalent thermal conductivity. This result is of great interest since the measurement of the equivalent conductivity of low-density thermal insulators is a major problem in the field of thermal characterisation.

Numerical results also demonstrated that the fact that real probes present thermal characteristics (either thermal inertia ($\rho_{Ni}.C_{Ni}$) ($\rho_{Ka}.C_{Ka}$) or thermal conductivity k_{Ni}, k_{Ka}) noticeably different from the thermal insulators tested disturbs noticeably the thermograms recorded. The identification procedure succeeds in fitting satisfactorily the thermal response by identifying noticeable temperature shift and time correction. However, when the thermal inertia of the material is too different from the probe, the thermal conductivity and thermal inertia identified are likely to deviate from the exact values. This is particularly the case for low-density XPS foams whose thermal inertia ($\rho.C$) is almost 2 order of magnitude lower than ($\rho_{Ni}.C_{Ni}$) and ($\rho_{Ka}.C_{Ka}$). In this case, the relative errors on k and ($\rho.C$) can exceed 10%. Lower errors are found for insulating materials with larger thermal inertia such as silica aerogel. Anyway, the validity of the present method is, in these cases, questionable.

The hot-disk measurements conducted on a reference XPS foam sample and a silica aerogel using a standard hot-disk apparatus confirms this latest conclusion since significant errors in the estimation of the thermal inertia are found for both materials whereas the errors on the thermal conductivity remain acceptable.

This current limitation of the use of the classical Hot-Disk method for insulating materials may certainly be overcome by developing an improved identification procedure. In addition to the parameters A and t_c used in the classical method, this new procedure would resort to one or more additional parameters allowing to reproduce faithfully the disturbance and to identify accurate values for both k and ($\rho.C$). This will be the subject of a coming publication.

Acknowledgments

This study is a contribution to the ANR Habisol 2009 project entitled “NANOCEL” (Project Number ANR-09-HABISOL-00 from 01-2010 to 01-2013). The authors acknowledge the partners of this project: the Neotim company, the EC2MS company, the ARMINES/CEP and ARMINES/CEMEF laboratories, the LFSM laboratory of CEA Pierrelatte, the GES Laboratory of the Montpellier II University, and the DMMC department of EDF.

References

[1] A. Degiovanni, M. Laurent, Nouvelle technique d'identification de la diffusivité thermique pour la méthode FLASH, Revue de Physique Appliquée 21 (3) (1986) 229–237 (English Abstract).
[2] O. Hahn, F. Raether, M.C. Arduini-Schuster, J. Fricke, A. Degiovanni, Transient coupled conductive/radiative heat transfer in absorbing, emitting and scattering media: application to laser-flash measurements on ceramic materials, International Journal of Heat and Mass Transfer 40 (3) (1997) 689–698.
[3] M. Lazard, S. André, D. Maillet, Diffusivity measurement of semi-transparent media: model of the coupled transient heat transfer and experiments on glass, silica glass and zinc selenide, International Journal of Heat and Mass Transfer 47 (2004) 477–487.
[4] R. Coquard, J. Randrianalisoa, S. Lallich, D. Baillis, Extension of the FLASH method to semi-transparent polymer foams, Journal of Heat Transfer ASME 133 (9) (2011).
[5] B. Ladevie, Mise au point de dispositifs de caractérisation thermophysique de matériaux ioslants solides ou pâteux. Extension aux fluides cisaillés, ENSAM Bordeaux, 1998.
[6] J.P. Laurent, Optimisation d'outils de mesure in situ des paramètres thermiques: Application au matériau TERRE, INPG Grenoble, 1986.
[7] E. Coment, J.-C. Batsale, B. Ladevie, J.-L. Battaglia, A simple device for determining thermal effusivity of thin plates, High Temperatures – High Pressures 34 (6) (2002) 627–637.
[8] R. Coquard, D. Baillis, D. Quenard, Experimental and theoretical study of the hot-wire method applied to low-density thermal insulators, International Journal of Heat and Mass Transfer 49 (23–24) (2006) 4511–4524.
[9] M. Gustavsson, E. Karawacki, S.E. Gustafsson, Thermal conductivity, thermal diffusivity and specific heat of thin samples from transient measurements with hot-disk sensors, Review of Scientific Instruments 65 (1994) 3856–3859.
[10] S.E. Gustafsson, Transient plane source techniques for thermal conductivity and thermal diffusivity measurements of solid materials, Review of Scientific Instruments 62 (1991) 797–804.
[11] V. Bohac, M.K. Gustavsson, L. Kubicar, S.E. Gustafsson, Parameter estimations for measurements of thermal transport properties with the hot disk thermal constants analyser, Review of Scientific Instruments 71 (2000) 2452–2455.
[12] S. Malinaric, Parameter estimation in dynamic plane source method, Measurement Science and Technology 15 (2004) 807–813.
[13] Y. He, Rapid thermal conductivity measurement with a hot disk sensor: part 1. Theoretical considerations, Thermochimica Acta 436 (2005) 122–129.
[14] S.A. Al-Ajlan, Measurements of thermal properties of insulation materials by using transient plane source technique, Applied Thermal Engineering 26 (2006) 2184–2191.
[15] Y. Jannot, Z. Acem, A quadrupolar complete model of the hot disc, Measurement Science and Technology 18 (2007) 1229–1234. http://dx.doi.org/10.1088/0957-0233/18/5/009.
[16] M. Gustavsson, S.E. Gustafsson, Thermal conductivity as an indicator of fat content in milk, Thermochimica Acta 442 (2006) 1–5.
[17] M. Gustavsson, S.E. Gustafsson, Thermal Conductivity 27, DEStech Pubs. Inc., Lancaster, Pennsylvania, 2003, 338–346.
[18] R. Coquard, D. Baillis, D. Quenard, Experimental and theoretical study of the hot-ring method applied to low-density thermal insulators, International Journal of Thermal Sciences 47 (3) (2008) 324–338.
[19] B.G. Carlson, K.D. Lathrop, Transport theory – the method of discrete ordinates, in: H. Greenspan, C.N. Kelber, D. Okrent (Eds.), Computing Methods in Reactor Physics, Gordon and Breach, New-York, 1968, pp. 165–266.
[20] S. Jendoubi, H.S. Lee, T.-K. Kim, Discrete ordinates solution for radiatively participating media in a cylindrical enclosure, Journal of Thermophysics and Heat Transfer 7 (1993) 213–219.
[21] M.Y. Kim, S.W. Baek, Modeling of radiative heat transfer in an axisymmetric cylindrical enclosure with participating medium, Journal of Quantitative Spectroscopy and Radiative Transfer 90 (2005) 377–388.
[22] L.H. Liu, T. He-Ping, Transient radiation and conduction in a two-dimensional participating cylinder subjected to a pulse irradiation, International Journal of Thermal Science 40 (2001) 877–889.
[23] C.Y. Wu, N.R. Ou, et al., Transient two dimensional radiative and conductive heat transfer in an axisymmetric medium, Heat and Mass Transfer 33 (1998) 327–331.
[24] G. Jeandel, P. Boulet, G. Morlot, Radiative transfer through a medium of silica fibres oriented in parallel planes, International Journal of Heat and Mass Transfer 36 (2) (1993) 531–536.
[25] R. Coquard, D. Baillis, D. Quenard, Radiative properties of expanded polystyrene foams, Journal of Heat Transfer 131 (1) (2009) 012702.
[26] R. Coquard, D. Baillis, D. Rochais, Experimental investigations of the coupled conductive and radiative heat transfer in metallic/ceramic foams, International Journal of Heat and Mass Transfer 52 (21–22) (2009) 4907–4918.